The Spo7 sequence LLI is required for Nem1-Spo7/Pah1 phosphatase cascade function in yeast lipid metabolism

Mona Mirheydari, Prabuddha Dey, Geordan J. Stukey, Yeonhee Park, Gil-Soo Han, and George M. Carman*

From the Department of Food Science and the Rutgers Center for Lipid Research, New Jersey Institute for Food, Nutrition, and Health, Rutgers University, New Brunswick, New Jersey, USA

Edited by F. Peter Guengerich

The Nem1-Spo7 complex in the yeast *Saccharomyces cerevisiae* is a protein phosphatase that catalyzes the dephosphorylation of Pah1 phosphatidate phosphatase, required for its translocation to the nuclear/endoplasmic reticulum membrane. The Nem1–Spo7/Pah1 phosphatase cascade plays a major role in triacylglycerol synthesis and in the regulation of phospholipid synthesis. In this work, we examined Spo7, a regulatory subunit required for Nem1 catalytic function, to identify residues that govern formation of the Nem1-Spo7 complex. By deletion analysis of Spo7, we identified a hydrophobic Leu-Leu-Ile (LLI) sequence comprising residues 54–56 as being required for the protein to complement the temperature-sensitive phenotype of an *spo7Δ* mutant strain. Mutational analysis of the LLI sequence with alanine and arginine substitutions showed that its overall hydrophobicity is crucial for the formation of the Nem1-Spo7 complex as well as for the Nem1 catalytic function on its substrate, Pah1, *in vivo*. Consistent with the role of the Nem1–Spo7 complex in activating the function of Pah1, we found that the mutational effects of the Spo7 LLI sequence were on the Nem1–Spo7/Pah1 axis that controls lipid synthesis and related cellular processes (*e.g.* triacylglycerol/phospholipid synthesis, lipid droplet formation, nuclear/endoplasmic reticulum membrane morphology, vacuole fusion, and growth on glycerol medium). These findings advance the understanding of Nem1-Spo7 complex formation and its role in the phosphatase cascade that regulates the function of Pah1 phosphatidate phosphatase.

In the model eukaryote *Saccharomyces cerevisiae* (in this paper, "yeast" is used interchangeably with *Saccharomyces cerevisiae*), the lipid intermediate phosphatidic acid (PA) is used for the synthesis of phospholipids and the neutral lipid triacylglycerol (TAG) (1–4) (Fig. 1). The bifurcation of PA to these lipids is governed by the demands of cell growth and metabolism (1–4). For example, PA is primarily metabolized into phospholipids via CDP-diacylglycerol (CDP-DAG) (1–4) during logarithmic growth when phospholipids are needed for membrane synthesis, metabolic process, and cellular signaling (Fig. 1). However, as cells progress into stasis (*e.g.* stationary phase), PA is primarily metabolized into TAG via diacylglycerol (DAG) (1–4). (Mutants defective in the CDP-DAG-dependent synthesis of phosphatidylcholine and/or phosphatidylethanolamine may synthesize these phospholipids from DAG via the CDP-choline and/or CDP-ethanolamine branches of the Kennedy pathway when supplemented with choline and/or ethanolamine [5–7].) This metabolic switch is largely controlled by the Nem1-Spo7/Pah1 phosphatase cascade (1–4, 8, 9) (Fig. 1).

Pah1 has the molecular function of PA phosphatase (10), which produces DAG by the dephosphorylation of PA (11, 12) (Fig. 1). The enzyme is a phosphoprotein in the cytosol, with its phosphorylation catalyzed by multiple protein kinases (13–18) on at least 40 serine/threonine residues (19–30) (Fig. 2). Overall, the phosphorylation of Pah1 causes its localization in the cytosol and prevents its access to the endoplasmic reticulum (ER) membrane-associated substrate PA, and has the effect of reducing its catalytic activity (13–16, 20). The ER membrane-resident protein phosphatase complex (31), consisting of Nem1 (catalytic subunit) and Spo7 (regulatory subunit), recruits and dephosphorylates Pah1 at the membrane surface and stimulates its PA phosphatase activity (20, 32–34) (Fig. 1). Compared with unphosphorylated/dephosphorylated Pah1, its phosphorylated form is more stable against degradation by the 20S proteasome (35, 36), except that it becomes more sensitive to the proteasomal degradation upon phosphorylation by protein kinase C (16). Like its substrate, Pah1, the Nem1-Spo7 phosphatase complex is regulated by phosphorylation (30, 37–41) (Fig. 2). For example, its phosphorylation by protein kinases A (40) and C (41) affects the function of the Nem1-Spo7/Pah1 axis for the decrease and increase, respectively, of TAG synthesis.

The activities of Pah1 PA phosphatase (10, 42) and Nem1 protein phosphatase (31, 43) are both dependent on the halo-acid dehalogenase (HAD)-like domain with the DXDX(T/V) catalytic motif (Fig. 2). For Pah1, in addition to the catalytic domain, its N-LIP domain is also important for PA phosphatase activity (42). Pah1 is a peripheral membrane protein that translocates to the ER membrane via its dephosphorylation by the Nem1-Spo7 complex. For Pah1 translocation, its acidic tail at the C terminus is required to interact with the Nem1-Spo7 phosphatase complex (33), whereas its amphipathic helix at the N terminus is crucial to associate with the membrane surface (32). The tryptophan residue of Pah1 in the conserved sequence WRDPLVDID is essential for its *in vivo* function but is not required for catalytic activity (44). Nem1 and Spo7, which form a protein phosphatase complex, are integral membrane proteins, both of which contain two transmembrane domains (31). The complex formation of Nem1 with Spo7 occurs through its C-terminal conserved domain (31). The interaction of Spo7 with Pah1 (38) facilitates the formation of an enzyme-substrate complex between Nem1 and Pah1 (33).

---

* For correspondence: George M. Carman, gcarman@rutgers.edu.

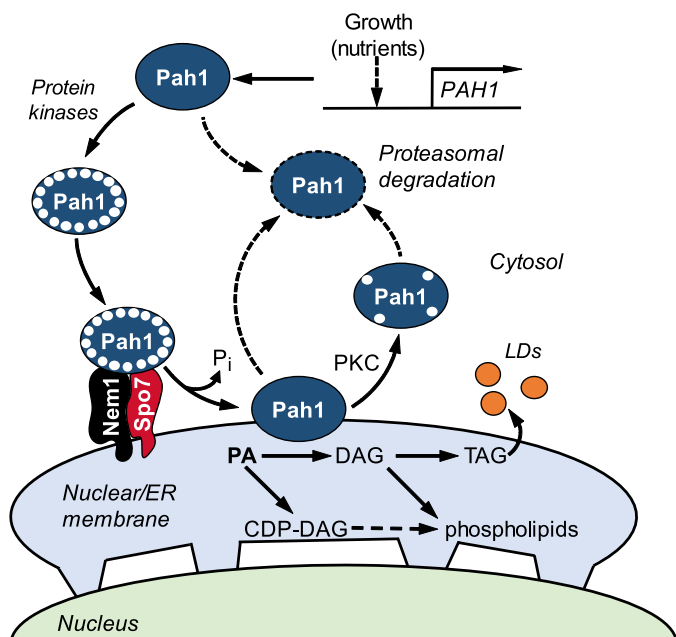## Spo7 sequence LLI is required for Nem1-Spo7/Pah1 function

Figure 1. Model for Pah1 localization and stability regulated by phosphorylation and dephosphorylation and for its role in lipid synthesis. The expression of *PAH1* is regulated during growth by nutrient status as mediated by the Opi1/Ino2-Ino4 (Henry) regulatory circuit and transcription factors Gis1, Rph1, and Zap1 (48, 109). Pah1 is phosphorylated (small *white circles*) by multiple protein kinases in the cytosol and translocates to the nuclear/ER membrane through its dephosphorylation by the Nem1-Spo7 complex (31, 32). Dephosphorylated Pah1 that is associated with the nuclear/ER membrane via its amphipathic helix (32) catalyzes the conversion of PA to DAG (10), which is converted to TAG for storage in lipid droplets (*LDs*). The DAG is also used for the synthesis of phosphatidylcholine or phosphatidylethanolamine via the Kennedy pathway when cells are supplemented with choline or ethanolamine (7, 110). Unphosphorylated/dephosphorylated Pah1 or protein kinase C (*PKC*)-phosphorylated Pah1 (16) is degraded by the 20S proteasome (indicated by the *dashed-line arrows*) (36).

In the present work, we examined the structural requirement of Spo7 in regulating the function of the Nem1-Spo7/Pah1 phosphatase cascade. Deletion analysis of Spo7 indicated that its amino acid region 46–65 is required for Nem1-Spo7/Pah1 axis function, and the N-terminal region contains the hydrophobic sequence Leu-Leu-Ile (LLI) (residues 54–56), conserved in fungi. Mutational analysis showed that the overall hydrophobicity of the LLI sequence is required for the complex formation of Spo7 with Nem1, and its defect causes a significant loss of the phosphatase complex-controlled Pah1 function (*e.g.* TAG synthesis and lipid droplet formation, the nuclear/ER membrane morphology, vacuole fusion, and growth at elevated temperature and on glycerol as a carbon source).

Results

Identification of Spo7 LLI sequence as a functional requirement

To assess the structural requirement of Spo7 for its function, we mutated the 5′ coding region of *SPO7* to produce the nested deletions of the protein from the N terminus (Table 1). The mutant alleles of *SPO7* on a low-copy-number plasmid were transformed into the *spo7Δ* mutant and evaluated for their ability to complement the mutant phenotypes. Loss of Spo7, like that of Pah1 or Nem1, renders cells defective in growth at 37 °C

(Fig. 3) (10, 31, 43, 45). Accordingly, we first examined whether the N-terminally truncated forms of Spo7 complement the growth defect of the *spo7Δ* mutant (Fig. 3). Like the full-length Spo7, its truncation forms Spo7Δ(2–25) and Spo7Δ(2–45) complemented the *spo7Δ* temperature-sensitive phenotype. However, the expression of Spo7Δ(2–65) did not complement the mutant phenotype. These results indicate that the loss of Spo7 function is caused by the lack of its sequence consisting of amino acids 46 to 65. A protein Blast analysis of the Spo7 sequence revealed the amino acid stretches that are conserved in fungi. We focused on one stretch, namely, LLI (residues 54–56), with the notion that hydrophobic interactions (46) govern the formation of the Nem1-Spo7 phosphatase complex. To examine this possibility, we constructed the *SPO7* allele whose product lacks only the LLI sequence. The expression of the LLI-deficient Spo7, Spo7Δ(54–56), did not complement the *spo7Δ* temperature-sensitive phenotype (Fig. 3), showing that the hydrophobic sequence is required for Spo7 function.

We next examined the importance of the hydrophobicity of the LLI sequence by mutating each individual amino acid to alanine and arginine. The alanine substitution conserves the hydrophobic property of the leucine and isoleucine residues, whereas the arginine substitution introduces the hydrophilic property instead. The expression of the alanine-substituted forms (*i.e.* L54A, L55A, and I54A) of Spo7 complemented the *spo7Δ* temperature-sensitive phenotype (Fig. 3). In contrast, the arginine-substituted forms did not complement (L54R and L55R) or weakly complemented (I56R) the *spo7Δ* temperature sensitivity (Fig. 3). These results indicate that the hydrophobic property of the LLI sequence is important for Spo7 function, and that the hydrophobic requirement is more stringent for the leucine residues.

Spo7 LLI sequence interacts with Nem1

Spo7 functions as a regulatory subunit of the Nem1-Spo7 phosphatase complex (31, 43). To address the hypothesis that the LLI sequence is required for the protein–protein interaction of Spo7 and Nem1, we examined the mutational effects of the hydrophobic sequence on Nem1-Spo7 complex formation. In this analysis, the isolation of the phosphatase complex and its immunodetection were facilitated by using the protein A-tagged Nem1 and the Myc-tagged Spo7 (20, 31, 34, 40), which are functional to complement the *spo7Δ* phenotypes (*e.g.* temperature sensitivity and growth defect on glycerol medium).

The presence of Nem1-PtA in the isolated complex could be determined by immunoblot analysis with anti-protein A or anti-Nem1 antibody. However, anti-protein A antibody was more robust in signal detection; thus, it was used in this analysis. The cross-reactivity of anti-Spo7 antibody with proteins whose electrophoretic mobility overlaps that of untagged Spo7 interfered with the detection of the Spo7-specific signal. To circumvent this problem, we utilized the Myc-tagged version of Spo7 (31) that exhibits slower electrophoretic mobility for clear analysis with anti-Spo7 antibody. Although anti-Myc antibody detected Spo7-Myc, its signal was not as robust as that detected with anti-Spo7 antibody. Nem1 and Spo7 are very-low-abundance proteins (47), and their detection from cell extracts was
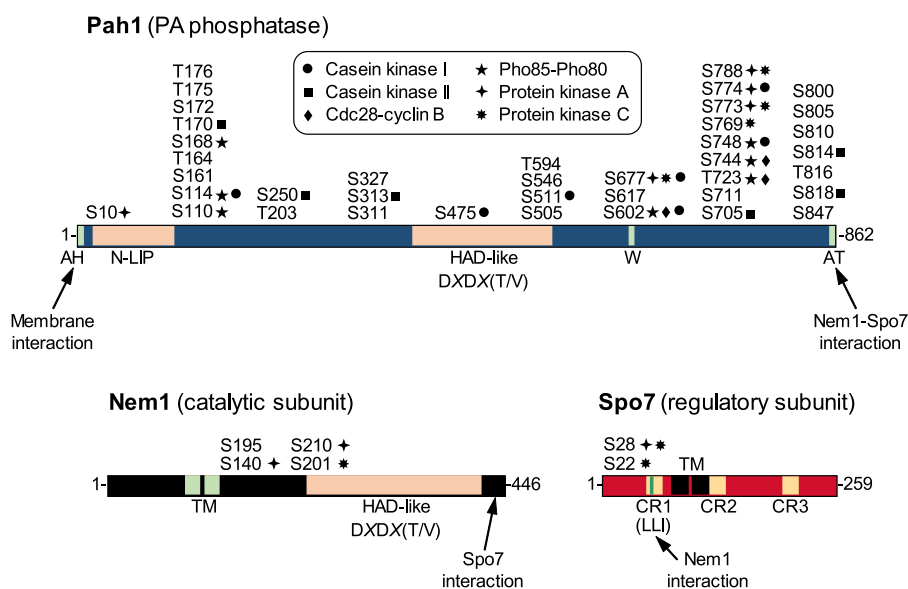
Figure 2. Schematic diagrams for the domains/regions and phosphorylation sites of Pah1, Nem1, and Spo7. The diagram of Pah1 denotes the positions of the amphipathic helix (*AH*) required for membrane interaction (32), the N-LIP and HAD-like domains required for PA phosphatase activity (42), the tryptophan (*W*) residue within the C-terminal conserved sequence, WRDPLVDID, required for function *in vivo* (44), and the acidic tail (*AT*) required for interaction with the Nem1-Spo7 complex (33). The serine (*S*) and threonine (*T*) residues known to be phosphorylated (19–30) are grouped at their approximate positions and marked for the responsible protein kinases, including casein kinase I (18), casein kinase II (17), Cdc28-cyclin B (13), Pho85-Pho80 (11), protein kinase A (15), and protein kinase C (16). For Nem1, the diagram denotes the HAD-like domain required for protein phosphatase activity and the C-terminal region required for interaction with Spo7 (31). For Spo7, the diagram shows the conserved regions (*CR*) 1, 2, and 3 (*yellow*) and the LLI sequence (*green*) within CR1 required for interaction with Nem1 (this work). The transmembrane (*TM*) regions of Nem1 and Spo7 (31) and the serine residues phosphorylated by protein kinase A (40) or protein kinase C (41) are also indicated.

untenable by immunoblotting with available antibodies. Thus, the typical input (*i.e.* cell extract) control was not applicable to the Nem1–Spo7 interaction data presented here.

Nem1-PtA was affinity purified with IgG-Sepharose from the extracts of *NEM1-PtA spo7Δ* cells expressing Spo7-Myc, and its level was determined by immunoblot analysis with anti-protein A antibody (Fig. 4A). In addition, Spo7-Myc copurified with Nem1-PtA was detected by immunoblot analysis with anti-Spo7 antibody (Fig. 4A). The quantification of Spo7-Myc showed that the amounts of the alanine-substituted forms (*i.e.* L54A, L55A, and I56A) were similar to that of the WT protein (Fig. 4B). However, the levels of the arginine-substituted forms L54R, L55R, and I56R were greatly reduced by 93, 85, and 63%, respectively. This result suggested that the hydrophobicity of the LLI sequence is crucial for Spo7 to form a complex with Nem1. However, we cannot rule out the possibility that the arginine mutations caused reduced stability of the Spo7 protein.

For Nem1-PtA, its cellular levels were shown to correlate with the levels of copurified Spo7-Myc (Fig. 4B). Unlike the alanine-substituted forms (*i.e.* L54A, L55A, and I56A) of Spo7, its arginine-substituted forms, L54R, L55R, and I56R, had the effect of reducing the Nem1-PtA level by 78%, 80%, and 44%, respectively. Considering that the Nem1-PtA level is reduced by 85% in the cell lacking Spo7-Myc expression (*i.e.* vector control), this result raises the suggestion that Nem1 is unstable when it cannot form a complex with Spo7.

Spo7 LLI sequence is required for the Nem1 catalytic activity

The Nem1-Spo7 phosphatase complex catalyzes the dephosphorylation of native Pah1, which is shown by a small increase in its electrophoretic mobility in SDS-PAGE (13, 14, 20). In contrast, the phosphorylation of Pah1 at Ser-723, Ser-744, and Ser-748 by the Pho85-Pho80 protein kinase is shown by a small decrease in its migration in the polyacrylamide gel (13, 14, 20). The Pho85-Pho80-mediated phosphorylation in the cell is required to ensure that the localization of Pah1 to the membrane depends on its dephosphorylation by the Nem1-Spo7 phosphatase (20). Accordingly, we examined the Nem1-Spo7 phosphatase activity *in vivo* on the substrate Pah1 using its phosphorylation state, which is reflected by differential electrophoretic mobility (Fig. 5). Compared with the expression of Spo7 (*i.e.* WT), the lack of its expression (*i.e.* vector) resulted in the production of the slower-migrating form of Pah1 concomitant with the lack of its faster-migrating form, indicating that the Nem1-Spo7 phosphatase activity is required to dephosphorylate native Pah1.

The differential electrophoretic mobility of Pah1 was also shown from *spo7Δ* cells expressing the alanine- and arginine-substituted forms of Spo7 (Fig. 5). The faster-migrating form of Pah1 was shown from the expression of the L54A form, similar to the expression of WT Spo7. In contrast, the slower-migrating form of Pah1 was shown from the expression of the L54R form, similar to the lack of WT Spo7. Compared with the L54A form of Spo7, the L55A and I56A forms showed a less clear effect on producing the faster-migrating form of Pah1. However, the electrophoretic mobilities of Pah1 from the expression of L55A and I56A were shown to be faster than those from the expression of L55R and I56R. The L55R and I56R forms were similar to the L54R form in producing the slower-migrating form of Pah1.

The relative amounts of Pah1 from cells expressing the L54A, L54R, L55A, L55R, I56A, and I56R Spo7 mutant

Table 1
Strains and plasmids used in this work

Strain or plasmid	Genotype or relevant characteristics	Source or reference
Strains		
E. coli DH5α	F⁻ ψ80d*lacZ*ΔM15Δ (*lacZYA-argF*)U169 *deoR recA1 endA1 hsdR17*(r$_k^-$ m$_k^+$) *phoA supE44* λ⁻ *thi-1 gyrA96 relA1*	95
S. cerevisiae		
RS453	*MAT**a** ade2-1 his3-11,15 leu2-3,112 trp1-1 ura3-52*	93
Mutant derivatives		
GHY67	*spo7Δ::URA3*	40
GHY68	*NEM1-PtA spo7Δ::URA3*	40
SS1002	*nem1Δ::HIS3*	31
SS1026	*pah1Δ::TRP1*	43
Plasmids		
pRS415	Single-copy *E. coli*/yeast shuttle vector with *LEU2*	92
pGH443	*SPO7* inserted into pRS415	40
pGH443-Δ(2–25)	*SPO7* lacking residues 2–25	This study
pGH443-Δ(2–45)	*SPO7* lacking residues 2–45	This study
pGH443-Δ(2–65)	*SPO7* lacking residues 2–65	This study
pGH443-Δ(54–56)	*SPO7* lacking residues 54–56	This study
pGH443-L54A	*SPO7* with the L54A mutation	This study
pGH443-L54R	*SPO7* with the L54R mutation	This study
pGH443-L55A	*SPO7* with the L55A mutation	This study
pGH443-L55R	*SPO7* with the L54R mutation	This study
pGH443-I56A	*SPO7* with the I56A mutation	This study
pGH443-I56R	*SPO7* with the I56R mutation	This study
pRS314-*SPO7-Myc*	*SPO7-Myc* inserted into pRS314	31
pGH447	BamH1 site inserted before stop codon of *SPO7* in pGH443	This study
pGH448	3x*Myc* tag inserted into *SPO7* in pGH447	This study
pGH448-L54A	*SPO7-Myc* with the L54A mutation	This study
pGH448-L54R	*SPO7-Myc* with the L54R mutation	This study
pGH448-L55A	*SPO7-Myc* with the L55A mutation	This study
pGH448-L55R	*SPO7-Myc* with the L54R mutation	This study
pGH448-I56A	*SPO7-Myc* with the I56A mutation	This study
pGH448-I56R	*SPO7-Myc* with the I56R mutation	This study
YCplac33-*S.E.C63-GFP*	*SEC63-GFP* fusion inserted into the *CEN/URA3* vector	93
pGH449	*SEC63-GFP* fusion inserted into the pRS413 *CEN/HIS3* vector	This study

proteins were 92, 100, 87, 91, 99, and 100%, respectively, compared with that of cells expressing WT Spo7 (Fig. 5*B*). Thus, the Spo7 LLI mutations do not majorly affect the amounts of Pah1.

Mutational effects of Spo7 LLI on the Nem1-Spo7/Pah1 function

Yeast cells deficient in Pah1, Nem1, or Spo7 exhibit a variety of phenotypes, all of which are caused by the lack of Pah1 PA phosphatase activity in producing DAG (4). The most notable phenotypes of the mutants include a great reduction in TAG synthesis (Fig. 6) (10, 48) and lipid droplet formation (Fig. 7*A*) (49, 50), the aberrant expansion of the nuclear/ER membrane (Fig. 8*A*) (31, 42, 43), defective vacuole fusion (Fig. 9*A*) (51–53), and growth defect at elevated temperature (Fig. 3) (10, 43, 45) and on glycerol as a sole carbon source (Fig. 10*A*) (10, 42). Some of these phenotypes (*e.g.* aberrant nuclear/ER morphology or defective vacuole fusion) are less pronounced in the *spo7Δ* mutant than in the *pah1Δ* mutant (Figs. 8*A* and 9*A*) but strong enough to evaluate the mutational effects of the LLI sequence on cell physiology.

Effect on lipid content

Spo7 is required for the Nem1 catalytic activity, which in turn regulates the Pah1 function to produce DAG for TAG synthesis (10, 20, 32–34, 43, 48). Accordingly, we examined the effect of the site-specific mutations of the LLI sequence on lipid contents (Fig. 6). Lipids were analyzed from the [2-¹⁴C]acetate-labeled cells at the stationary phase of growth, when Pah1 PA

phosphatase activity is highest (10, 48, 50). Lack of Spo7 (*i.e.* vector control) caused a 92% decrease in the amount of TAG but a 96% increase in the amount of phospholipids. The altered lipid levels of *spo7Δ* cells were not restored by expressing the arginine-substituted forms (*i.e.* L54R, L55R, and I56R) of Spo7. However, the expression of the alanine-substituted forms L54A and L55A restored the altered lipid levels caused by the *spo7Δ* mutation. Interestingly, the I56A form of Spo7, which complemented the *spo7Δ* temperature-sensitive phenotype, showed a modest increase in the TAG level without restoring the phospholipid level. The differential effects shown by the I56A form supports the notion that a lower level of Pah1 PAP activity is sufficient to support cell growth at elevated temperature (44).

Effect on lipid droplet formation

Pah1 produces DAG that is acylated to TAG (10), which is then stored in lipid droplets (49). Since the Pah1-controlled production of TAG affects lipid droplet formation, we examined the mutational effects of the LLI sequence on the quantity of cellular lipid droplets (Fig. 7*B*). The *spo7Δ* cells expressing WT Spo7 contained an average of 9 lipid droplets in the stationary phase of growth, whereas the mutant cells lacking its expression showed a reduction of the lipid droplet number of 62%. Compared with the effect of the WT control, the arginine-substituted forms (*i.e.* L54R, L55R, and L56R) of Spo7 did not significantly increase the lipid droplet number of the *spo7Δ* cells. In contrast, the expression of the alanine-substituted forms L54A and L55A restored the lipid droplet number to 80% of the WT control. Similar to its effect on the TAG level,
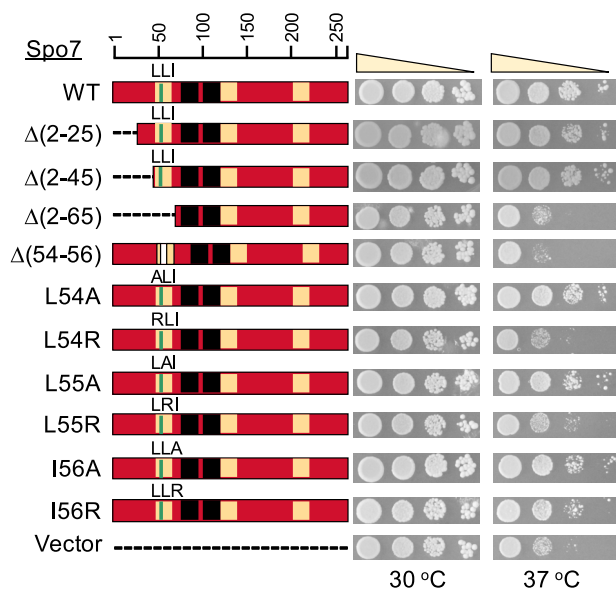
Figure 3. Identification of Spo7 LLI sequence as required for the Nem1-Spo7 function. The *spo7Δ* (GHY68) transformants expressing the indicated *SPO7* alleles (pGH443 and its derivatives) were grown to saturation at 30 ℃ in SC-Leu medium. The cultures were adjusted to an A_{600} of 0.7, serially diluted (10-fold), and spotted onto SC-Leu agar plates. The growth of the transformant cells on solid medium was scored after 3 days of incubation at 30 and 37 ℃. The data are representative of three independent experiments. The position of the amino acid residues from full-length Spo7 is shown (*top left*).

the I56A form showed a modest increase in the lipid droplet number to 58% of the WT control.

Effect on nuclear/ER morphology

The lack of Spo7, Nem1, or Pah1 in the cell is characterized by an irregularly shaped nucleus with the expansion of the nuclear/ER membrane (Fig. 8A) (31, 42, 43). This phenotype is attributed to the increased synthesis of membrane phospholipids as caused by the defect of the Nem1-Spo7/Pah1 phosphatase cascade (4, 9, 10, 43, 48, 54). Accordingly, we examined the mutational effects of the LLI sequence on the nuclear/ER morphology of the cell by the expression of the ER marker Sec63-GFP (Fig. 8B). On average, about 60% of *spo7Δ* cells exhibited aberrant nuclear/ER morphology compared with only 3.5% of WT cells. The expression of the alanine-substituted forms of Spo7 significantly reduced the aberrant nuclear/ER morphology of *spo7Δ* cells (14–22%), whereas the expression of the arginine-substituted forms had weaker effects on suppressing the mutant phenotype (37–42%).

Effect on vacuole fusion

A phenotype characteristic of the cell lacking Pah1, Nem1, or Spo7 is the appearance of fragmented vacuoles that fail to fuse upon nutrient limitation (Fig. 9A) (51, 53). Thus, we examined the effects of the site-specific mutations of the LLI sequence on the vacuole morphology of the cell by staining with FM 4-64. The defect of vacuole fusion was less pronounced in the *spo7Δ* mutant than in the *pah1Δ* or *nem1Δ* mutant (Fig. 9A, *lower*). As shown in Fig. 9B, about 18% of *spo7Δ* cells possessed fragmented vacuoles compared with 2.5% of the mutant cells expressing WT Spo7. The expression of the alanine-substituted forms of Spo7
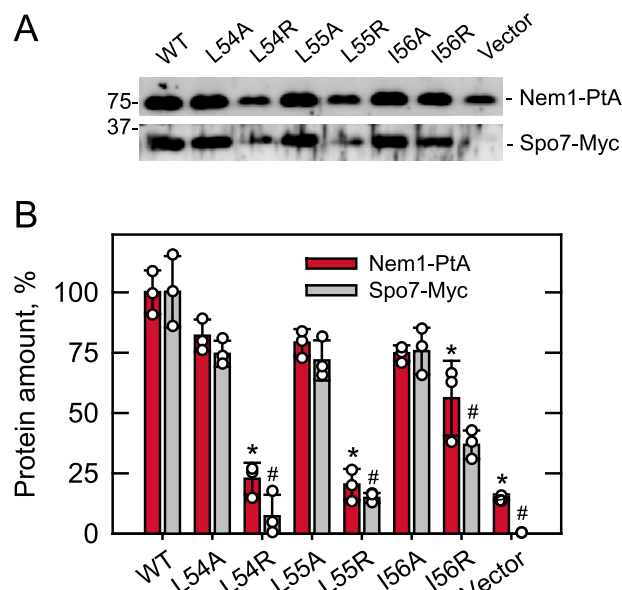

Figure 4. Nem1-Spo7 complex formation of *spo7Δ* cells expressing Spo7 with LLI mutations. *A*, the *spo7Δ* mutant (GHY68), which harbors chromosomal *NEM1-PtA*, was transformed with pGH448 and its derivatives for the expression of the WT and mutant forms of Spo7-Myc. The yeast transformants were grown at 30 ℃ in SC-Leu medium to the late logarithmic phase, and cell extracts were prepared. The cell extracts were adjusted to a protein concentration of 2.5 mg/ml and incubated with IgG-Sepharose. The affinity resins were precipitated, washed, and treated with the Laemmli sample buffer. After centrifugation, the affinity-purified proteins in the supernatant were resolved by SDS-PAGE and transferred to a PVDF membrane. The membrane was cut at the 50-kDa position, and the upper portion was probed with anti-protein A antibody, whereas the lower portion was probed with anti-Spo7 antibody. The positions of Nem1-PtA, Spo7-Myc, and molecular mass standards are indicated. *B*, the signals of Nem1-PtA and Spo7-Myc in *panel A* were quantified by ImageQuant software. The levels of mutant Spo7-Myc were normalized to the level (set at 100%) of the WT protein; the levels of Nem1-PtA from the transformant cells expressing mutant Spo7-Myc were normalized to the protein level (set at 100%) from those expressing the WT protein. The density of a background region on the blot was subtracted from the density of the protein band of interest. The immunoblots in *panel A* are representative of three separate experiments, whereas the data in *panel B* are averages from the three experiments ± S.D. (*error bars*). The individual data points are also shown. *, $p < 0.05$ *versus* Nem1-PtA of cells expressing WT Spo7-Myc. #, $p < 0.05$ *versus* Spo7-Myc of cells expressing WT Spo7-Myc.

restored the defective vacuole fusion of *spo7Δ* cells to a level similar to that of the cells expressing the WT protein. In contrast, the expression of the arginine-substituted forms had little effect on restoring the defective vacuole fusion of *spo7Δ* cells (L54R, 15%; L55R, 15%; I56R, 12%).

Effect on growth with glycerol as the carbon source

Cells lacking Pah1 or Nem1 exhibited a growth defect when glycerol was substituted for glucose as a sole carbon source (Fig. 10A) (42, 45, 55). Because the Nem1-Spo7 complex regulates Pah1 function, we examined whether *spo7Δ* mutant cells utilize glycerol as a carbon source. The *spo7Δ* cells exhibited a subtle loss-of-growth phenotype when grown on the glycerol-containing medium; this phenotype was complemented by the expression of WT Spo7 (Fig. 10B). The alanine-substituted forms (*i.e.* L54A, L55A, and I56A) of Spo7 also complemented the growth defect of *spo7Δ* cells on glycerol medium. However, the arginine-substituted forms (*i.e.* L54R, L55R, and I56R) did not complement the *spo7Δ* defect in glycerol utilization.
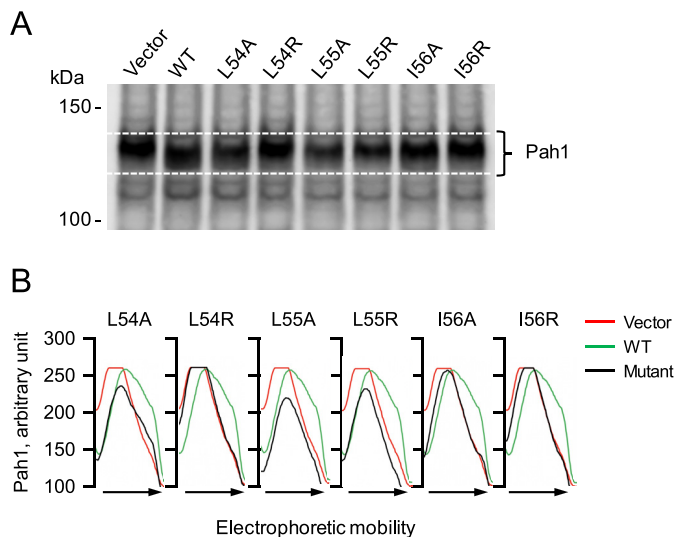
Figure 5. Electrophoretic mobility of Pah1 from *spo7*Δ cells expressing Spo7 with LLI mutations. The *spo7*Δ mutant (GHY67) was transformed with pGH443 and its derivatives for expression of the WT and mutant forms of Spo7-Myc. The yeast transformants were grown at 30 ℃ in SC-Leu medium to the mid-logarithmic phase. Cell extracts were prepared and subjected to SDS-PAGE (40 μg protein) using an 8% polyacrylamide gel. *A*, the proteins resolved in the polyacrylamide gel were transferred to a PVDF membrane and probed with anti-Pah1 antibody. The positions of Pah1 and molecular mass standards are indicated. The *white dashed line* is a guide to show the range in the electrophoretic mobility of Pah1 from the *spo7*Δ cells and those expressing WT Spo7. *B*, the signal intensities of Pah1 along its migration in the region between the *dashed white lines* in *panel A* were measured using the line graph function of ImageQuant software. The densitogram of Pah1 from the expression of mutant Spo7 (*black line*) was compared with those from the presence (*green line*) and absence (*red line*) of WT Spo7. The vector control and WT lines are included with each mutant protein for comparison. The data shown are representative of three separate experiments.
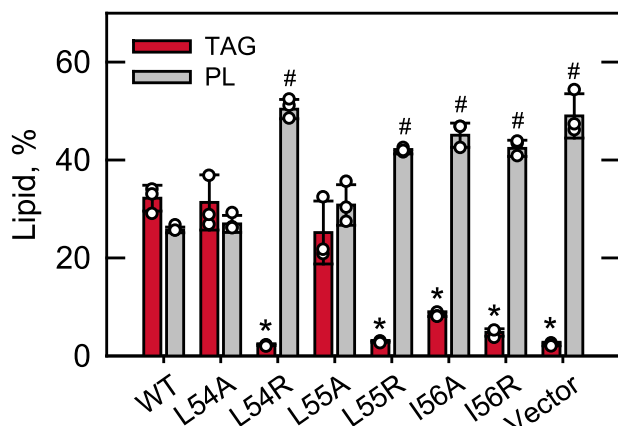

Figure 6. TAG and phospholipid levels of *spo7*Δ cells expressing Spo7 with LLI mutations. The *spo7*Δ mutant (GHY68) was transformed with pGH448 and its derivatives for expression of the WT and mutant forms of Spo7-Myc. The transformants were grown at 30 ℃ to stationary phase in SC-Leu medium containing [2-^{14}C]acetate (1 μCi/ml). Lipids were extracted from the radiolabeled cells, separated by TLC, subjected to phosphorimaging, and quantified by ImageQuant analysis. The levels of TAG and phospholipids (*PL*) were normalized to total chloroform-soluble lipids. The data are means ± S.D. (*error bars*) from three separate experiments. The individual data points are also shown. *, $p < 0.05$ *versus* TAG of WT. #, $p < 0.05$ *versus* phospholipid of WT.

Discussion

SPO7, which was originally identified as a gene involved in meiosis and sporulation (56), was shown to encode a protein

required to maintain a spherical nuclear morphology (31). The role of Spo7 in sporulation is unclear, but its role in the nuclear morphology is based on the formation of a protein phosphatase complex with Nem1 to regulate Pah1 PA phosphatase (20, 43). The dephosphorylation of Pah1 by the Nem1-Spo7 phosphatase at the nuclear/ER membrane (20, 32, 33) facilitates its membrane localization for catalytic activity on PA to produce DAG that is acylated to TAG (Fig. 1) (48). The storage lipid TAG is a reservoir for energy production as well as for growth resumption from stasis, and its synthesis protects cells against fatty acid–induced toxicity (50, 57–63). TAG production also has the effect of controlling the level of PA that is used for the *de novo* synthesis of membrane phospholipids. Accordingly, the disruption of the Nem1-Spo7/Pah1 phosphatase cascade by Spo7 deficiency causes the accumulation of PA that is exclusively converted to membrane phospholipids. The elevated level of PA also upregulates the production of phospholipid synthesis enzymes at the transcriptional level through the derepression of enzyme gene expression (10, 43, 48, 50, 54, 64). These changes lead to a massive increase in the level of phospholipids at the nuclear/ER membrane, causing the organelle membrane to be irregularly expanded. The lack of the Spo7-mediated control of the Nem1-Spo7/Pah1 phosphatase cascade also causes defects in other cellular processes (*e.g.* lipid droplet formation, vacuole fusion, and growth at elevated temperature and on glycerol medium) that are dependent on the regulatory function of PA and/or DAG.

In the Nem1-Spo7 phosphatase complex, Spo7 is a regulatory subunit for the function of the Nem1 catalytic subunit (31, 34, 38, 43, 65) and associates with its HAD-like domain (*i.e.* catalytic domain) at the C-terminal region (Fig. 2) (31). The work presented here is consistent with the notion that the LLI sequence of Spo7 at the N-terminal region is required for complex formation, and that the overall hydrophobicity of the amino acid residues is crucial for the protein-protein interaction with Nem1. It has been known that residue hydrophobicity is a dominant factor for protein–protein interactions (66). Thus, our findings indicate that the LLI-mediated hydrophobic interaction is a key factor for the formation of the Nem1-Spo7 complex. This mechanism of complex formation could be further supported by the identification of hydrophobic residues in the Nem1 catalytic domain that directly interact with Spo7 LLI. Obviously, the interaction of Spo7 with Nem1 would be better understood from the molecular structural information of the protein complexes. Our results also showed that Nem1 is unstable without forming a complex, indicating that Spo7 is required not only for the function of the catalytic subunit but also for its protein stability. The effect of complex formation on the stability of the catalytic subunit is conserved, as shown by the instability of human CTDNEP1 (catalytic subunit, also called Dullard) in the absence of complex formation with NEP1-R1 (regulatory subunit, also called TMEM188) (65, 67).

The orthologous components of the yeast Nem1-Spo7/Pah1 phosphatase cascade in higher eukaryotes consist of the CTDNEP1–NEP1-R1 complex (65, 67) and lipin PA phosphatase (10, 68–70). Like yeast Pah1, mammalian lipin is controlled for its localization and PA phosphatase activity (71–74) by phosphorylation (75–81) and dephosphorylation (65, 67, 82).
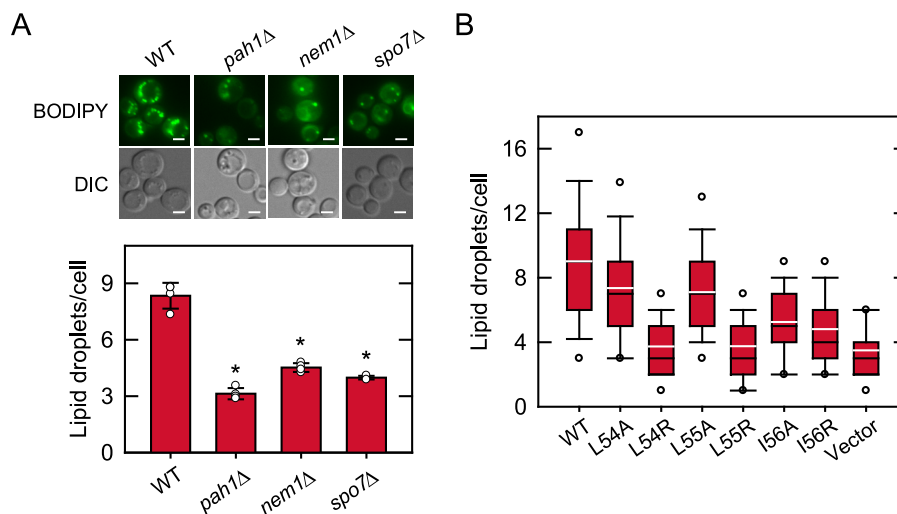
Figure 7. Lipid droplet formation of cells defective in the Nem1-Spo7/Pah1 phosphatase cascade and of *spo7Δ* cells expressing Spo7 with LLI mutations. *A*, WT, *pah1Δ*, *nem1Δ*, and *spo7Δ* cells were grown at 30 ℃ in SC medium to stationary phase and stained with BODIPY 493/503. *B*, *spo7Δ* (GHY68) transformants expressing the indicated *SPO7* allele (pGH443 and its derivatives) were grown and stained as in *panel A*, except that SC-Leu medium was used for plasmid selection. The stained lipid droplets were visualized by fluorescence microscopy, and the number of lipid droplets was counted from ≥4 fields of view (≥200 cells). *A*, *upper*, the images shown are representative of multiple fields of view. *DIC*, differential interference contrast. *White bar*, 2 μm. *A*, *lower*, the data shown are averages from three experiments ± S.D. (*error bars*). The individual data points are also shown. *, $p < 0.05$ *versus* cells expressing the WT control. *B*, the data are presented by the box plot. The *black* and *white lines* are the median and mean values, respectively, and the *white circles* are the outlier data points of the 5th and 95th percentiles.
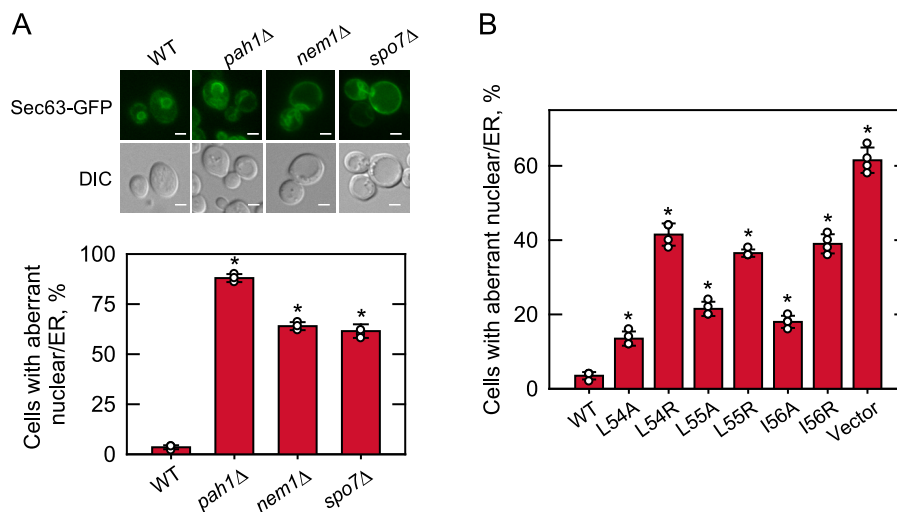

Figure 8. Nuclear/ER morphology of cells defective in the Nem1-Spo7/Pah1 phosphatase cascade and of *spo7Δ* cells expressing Spo7 with LLI mutations. *A*, WT, *pah1Δ*, *nem1Δ*, and *spo7Δ* cells harboring YCplac111-*SEC63-GFP* were grown at 30 ℃ in SC-Leu medium to logarithmic phase, and the fluorescence signal of the GFP-tagged ER marker Sec63 was visualized by fluorescence microscopy. *B*, *spo7Δ* (GHY68) transformants harboring pRS413-*SEC63-GFP* (pGH449) and the indicated *SPO7* allele (pGH443 and its derivatives) were grown and examined as in *panel A*, except that SC-His-Leu medium was used for plasmid selection. The percentage of cells with aberrant nuclear/ER morphology (misshaped *versus* round nuclei) was determined from ≥4 fields of view (≥200 cells). *A*, *upper*, the images shown are representative of multiple fields of view. *DIC*, differential interference contrast. *White bar*, 2 μm. *A*, *lower*, and *B*, the data shown are averages from three experiments ± S.D. (*error bars*). The individual data points are also shown. *, $p < 0.05$ *versus* cells expressing the WT control.

In addition, the loss of lipin PA phosphatase is responsible for a variety of lipid-based metabolic disorders. Lipin 1 deficiency in mice and humans causes rhabdomyolysis (83, 84), and its deficiency in mice is also characterized by hepatic steatosis during the neonatal period, lipodystrophy, insulin resistance, and peripheral neuropathy (68, 85). The polymorphism of human *LPIN1* is associated with insulin resistance and the metabolic syndrome (86). The deficiency of lipin 2 in humans results in chronic recurrent multifocal osteomyelitis and congenital dys-erythropoietic anemia (87, 88), whereas the specific polymorphisms of human *LPIN2* are associated with type 2 diabetes (89). In mouse small intestine, lipin 2 and lipin 3 deficiencies disrupt phospholipid homeostasis, impairing lipoprotein biogenesis and secretion (90). In mice, the loss of CTDNEP1 causes hemorrhagic ovarian cysts with the accumulation of red blood cells in follicles, leading to infertility (91). Unlike CTDNEP1, NEP1-R1 is not yet known for the effects of its deficiency. Nonetheless, the conservation of the phosphatase
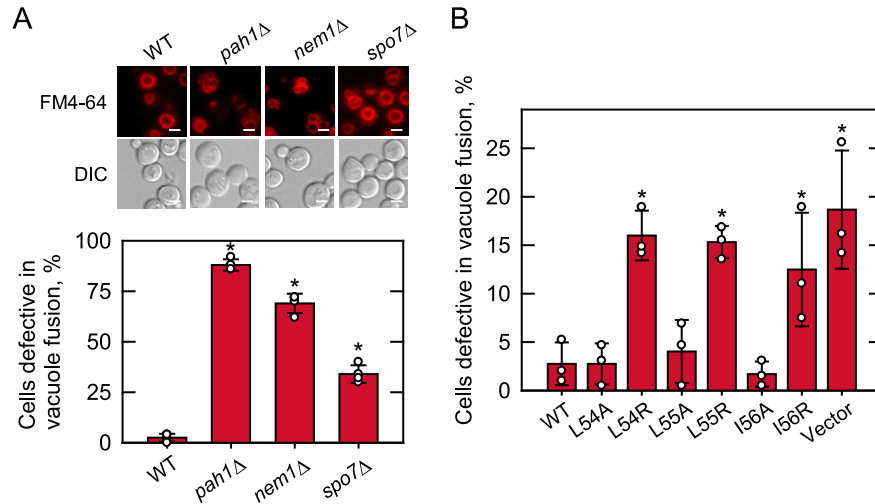
Figure 9. Vacuole morphology of cells defective in the Nem1-Spo7/Pah1 phosphatase cascade and of *spo7Δ* cells expressing Spo7 with LLI mutations. WT, *pah1Δ*, *nem1Δ*, and *spo7Δ* mutant cells were grown at 30 ℃ in SC medium to late-logarithmic phase, stained with FM4-64, and examined for vacuole staining by fluorescence microscopy. *B*, *spo7Δ* (GHY68) transformants expressing the indicated *SPO7* allele (pGH443 and its derivatives) were grown and stained as in *panel A*, except that SC-Leu medium was used for plasmid selection. The percentage of cells defective in vacuole fusion (*e.g.* fragmented vacuoles) was determined from ≥4 fields of view (≥200 cells). *A*, *upper*, the images shown are representative of multiple fields of view. *DIC*, differential interference contrast. *White bar*, 2 μm. *A*, *lower*, and *B*, the data shown are averages from three experiments ± S.D. (*error bars*). The individual data points are also shown. *, $p < 0.05$ *versus* cells expressing the WT control.
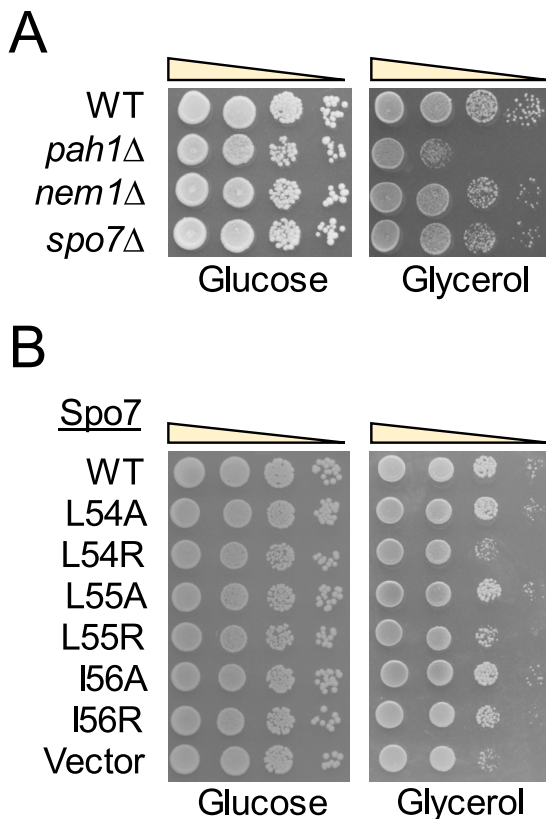

Figure 10. Glycerol utilization of cells defective in the Nem1-Spo7/Pah1 phosphatase cascade and of *spo7Δ* cells expressing Spo7 with LLI mutations. *A*, WT, *pah1Δ*, *nem1Δ*, and *spo7Δ* mutant cells were grown at 30 ℃ in YPD to saturation, serially diluted (10-fold), and spotted onto agar plates containing 2% glucose or 3% glycerol. *B*, *spo7Δ* (GHY67) transformants expressing the indicated *SPO7* allele (pGH443 and its derivatives) were grown in SC-Leu medium and treated as in *panel A*. Growth on glucose and glycerol was scored after 3 and 6 days, respectively, of incubation at 30 ℃. The data are representative of three independent experiments.

cascade indicates that an important avenue of inquiry is to understand how NEP1-R1 interacts with CTDNEP1 for the regulation of lipin activity.

Spo7 is conserved in eukaryotes from fungi to humans (65) by containing two transmembrane-spanning domains (TM1 and TM2) and three homology regions (CR1, CR2, and CR3) (Fig. 2). Whereas the LLI sequence contained within CR1 is conserved in fungi, the two amino acid residues following the first conserved leucine vary in higher eukaryotes (65). Moreover, the second amino acid in the sequence of the worm *Caenorhabditis elegans* (LKF), the fly *Drosophila melanogaster* (LKA), and the human *Homosapiens* (LKA) is the charged amino acid lysine. Thus, based on the data from yeast Spo7, its orthologs containing the lysine residue following the conserved leucine residue are likely to have a weak interaction with the Nem1 orthologs in those organisms.

Compared with CR1 located at the N-terminal region, CR2 and CR3 are located at the C-terminal region. The N-terminal CR1 and the C-terminal CR2/CR3, which are outside the transmembrane regions, are both oriented to the cytosol. The requirement of Spo7 as a regulatory subunit for the catalytic function of Nem1 is thought to be in the recruitment of the substrate. This function of Spo7 requires a region interacting with Pah1, which is separate from a region required to form a complex with Nem1. The LLI sequence of Spo7 located in the N-terminal CR1 is required to form a complex with Nem1. Thus, it is possible that CR2 and CR3 are involved in the recognition of Pah1. In this regard, work is currently in progress to assess the role of CR2 and CR3 in the interaction with Pah1.

Experimental procedures

Materials

Avanti Polar Lipids was the source of lipid standards. Bio-Rad supplied the molecular mass protein standards and

reagents for electrophoresis, immunoblotting, and protein determination. DNA size standards were from Invitrogen. Carrier DNA for yeast transformation was from Clontech. Growth media were from Difco Laboratories. GE Healthcare was the source of IgG-Sepharose, polyvinylidene difluoride (PVDF) membrane, and the enhanced chemifluorescence Western blotting detection kit. FM 4-64 was purchased from Molecular Probes, Inc. Millipore-Sigma was the supplier of ampicillin, BSA, 2-mercaptoethanol, PCR primers, nucleotides, Ponceau S stain, Triton X-100, protease and phosphatase inhibitors, rabbit anti-protein A antibody (product P3775, lot 025K4777), rabbit anti-myc antibody (product no. SAB4301136, lot no. 802535536), and silica gel 60 TLC plates. Enzyme reagents for DNA manipulations and the Q5 site-directed mutagenesis kit were obtained from New England Biolabs. Radiochemicals were from Perkin-Elmer Life Sciences, and scintillation-counting supplies were from National Diagnostics. Qiagen was the source of plasmid DNA purification kits. Thermo Scientific was the source of alkaline phosphatase-conjugated goat anti-rabbit IgG antibody (product 31340, lot NJ178812) and BODIPY 493/503. Anti-Nem1 (40), anti-Spo7 (40), and anti-Pah1 (13) antibodies were previously generated in New Zealand White rabbits. All other chemicals were reagent grade.

Strains, plasmids, and DNA manipulations

The strains and plasmids used in this work are listed in Table 1. *Escherichia coli* strain DH5α was used for plasmid maintenance and amplification. *S. cerevisiae* strains GHY67 (40) and GHY68 (40), which are *spo7Δ* mutants with chromosomal *NEM1* and *NEM1-PtA*, respectively, were used for the expression of plasmid-borne *SPO7* and its mutant derivatives. Plasmid pGH443 (40), which is a derivative of the *E. coli*/yeast shuttle vector pRS415 (92), directs the low-copy-number expression of *SPO7* in *S. cerevisiae.* Plasmid pGH447 was derived from pGH443 by introducing a BamHI site before the stop codon of *SPO7*. pGH448 was constructed from pGH447 by inserting a 126-bp BamHI fragment for the 3×Myc tag that was released from plasmid pRS314-*SPO7-Myc* (31). The derivatives of plasmids pGH443 and pGH448 with *SPO7* mutations were constructed by the Q5 site-directed mutagenesis kit with appropriate primers designed using the NEBaseChanger online software. pGH449 was constructed by ligation of the SmaI/SacI-digested pRS413 (92) with the *SEC63-GFP* DNA that was released from YCplac33-*SEC63-GFP* (93) by digestion with HindIII, treatment with Klenow fragment, and digestion with SacI. Standard methods were used for the isolation of chromosomal and plasmid DNA, for the digestion and ligation of DNA, and for the PCR amplification of DNA (94–96). Plasmid transformations of *E. coli* (95) and yeast (97) were performed as described previously. All gene mutations were confirmed by DNA sequencing.

Growth conditions

Bacterial cells were grown at 37 °C in lysogeny broth medium (1% tryptone, 0.5% yeast extract, 1% NaCl, pH 7.4). *E. coli* transformants containing plasmids were selected by antibiotic (*e.g.* 100 μg/ml ampicillin) resistance. Standard methods were used for culturing yeast (94, 95). Yeast cells were routinely grown at

30 °C in rich or synthetic complete medium, and those containing plasmids were maintained in synthetic dropout medium. Unless otherwise indicated, 2% glucose was included as a carbon source in growth medium. Solid media for the growth of *E. coli* and yeast contained agar at a concentration of 1.5 and 2%, respectively. For the measurement of growth on solid medium, serially diluted (10-fold) cultures were spotted onto agar medium, and cell growth was scored after incubation for 3 days at 30 or 37 °C (for temperature sensitivity). Growth on agar medium containing glycerol as the carbon source was scored after incubation for 6 days. Cell density in liquid cultures was estimated spectrophotometrically by measuring absorbance at 600 nm.

Preparation of cell extracts

All steps to prepare cell extracts were performed at 4 °C. Yeast cultures were harvested by centrifugation at $1,500 \times g$ for 5 min. The cells were washed with water and resuspended in lysis buffer (50 mM Tris-HCl [pH 7.5], 0.3 M sucrose, 10 mM 2-mercaptoethanol) containing protease inhibitors (0.5 mM phenylmethylsulfonyl fluoride, 1 mM benzamidine, 5 μg/ml aprotinin, 5 μg/ml leupeptin, and 5 μg/ml pepstatin) and phosphatase inhibitors (2 mM imidazole, 1 mM β-glycerophosphate, 1 mM sodium pyrophosphate, 1 mM sodium fluoride, and 1 mM sodium orthovanadate). The suspended cells were mixed with glass beads (0.5-mm diameter) and then disrupted by five repeats of a 1-min burst and 2-min cooling using a BioSpec Products Mini-Beadbeater-16 (98). The disrupted cells were centrifuged at $1,500 \times g$ for 10 min to separate cell extracts (supernatant) from unbroken cells and cell debris (pellet). The protein concentration of the cell extracts was determined by the method of Bradford (99) using BSA as a standard.

Isolation of the Nem1-Spo7 complex

The protein A-tagged Nem1-Spo7 complex was isolated from cell extracts (2 mg protein) by incubation overnight with IgG-Sepharose (10%, w/v, slurry). The complex was collected by centrifugation at $1,500 \times g$ for 30 s and washed three times with a modified radioimmune precipitation lysis buffer (50 mM Tris-HCl [pH 8.0], 150 mM NaCl, 1% Triton X-100, and 0.1% SDS) containing protease (0.5 mM phenylmethanesulfonyl fluoride, 1 mM benzamidine, 5 μg/ml aprotinin, 5 μg/ml leupeptin, and 5 μg/ml pepstatin) and phosphatase (10 mM sodium fluoride, 5 mM β-glycerophosphate, and 1 mM sodium vanadate) inhibitors (100). The Nem1 and Spo7 proteins were separated by SDS-PAGE (101) using 12% polyacrylamide gels and transferred to PVDF membrane (102–104).

Immunoblotting

Protein transfer from SDS-polyacrylamide gels to PVDF membranes was monitored by Ponceau S staining. The membrane blots were cut; the upper and lower portions were probed with rabbit anti-Nem1 (1 μg/ml) or rabbit anti-protein A (2 μg/ml) antibodies and with rabbit anti-Spo7 (1 μg/ml) or rabbit anti-Myc (1:1,000 dilution) antibodies, respectively. The immunoblot analysis of Pah1 from cell extracts subjected to SDS-PAGE using 8% polyacrylamide gels was performed with rabbit

anti-Pah1 antibody (2 μg/ml). The secondary goat anti-rabbit IgG antibody conjugated with alkaline phosphatase was used at a dilution of 1:5,000. Immune complexes on the PVDF membrane were detected using the enhanced chemifluorescence immunoblotting substrate. Fluorimaging, using a Storm 865 Molecular Imager (GE Healthcare), was used to acquire fluorescence signals from immunoblots, and the intensities of the images were analyzed by ImageQuant TL software (GE Healthcare). A standard curve was used to ensure that the immunoblot signals were in the linear range of detection.

Radiolabeling and analysis of lipids

The labeling of cellular lipids with $[2\text{-}^{14}\text{C}]$acetate was performed as described previously (105). Lipids were extracted (106) from the radiolabeled cells and then separated by one-dimensional TLC in the solvent system of hexane-diethyl ether-acetic acid (40:10:1, v/v) (107). The resolved lipids were visualized by phosphorimaging and quantified by ImageQuant TL software. The identity of radiolabeled lipids was confirmed by comparison with the migration of authentic standards visualized by staining with iodine vapor.

Fluorescence microscopy

For the fluorescent staining of lipid droplets, yeast cells were grown at 30 °C in synthetic medium to the stationary phase, incubated for 30 min with 2 μM BODIPY 493/503, washed with PBS (pH 7.4), and resuspended in the same buffer. For the fluorescent labeling of nuclear/ER membrane, yeast cells transformed with the *SEC63-GFP* plasmid (43) were grown at 30 °C in the selection medium to the logarithmic phase and subjected to microscopic analysis. For the fluorescent staining of vacuole membranes, cells were grown at 30 °C in synthetic medium to the late-logarithmic phase, incubated for 15 min at 30 °C with 32 μM FM 4-64, washed with yeast extract peptone dextrose, and resuspended in fresh growth medium (108). The number of lipid droplets per cell and the percentage of cells with aberrant nuclear/ER morphology (misshaped *versus* round nuclei) or defective vacuole fusion (*e.g.* fragmented vacuoles) were scored from ≥4 fields of view (≥200 cells). The green and red fluorescence signals were examined under a Nikon Eclipse Ni-U microscope with the EGFP/FITC/Cy2/AlexaFluor 488 and TRITC/Cy3/TagRFP/AlexaFluor 546 filters, respectively, re-corded by the DS-Qi2 camera, and subjected to imaging analysis with NIS-Elements BR software.

Analysis of data

Microsoft Excel software was used for the statistical analysis of data. *p* values of <0.05 were taken as significant differences.

Data availability

All data are contained within the manuscript.

References

1. Carman, G. M., and Han, G.-S. (2009) Phosphatidic acid phosphatase, a key enzyme in the regulation of lipid synthesis. *J. Biol. Chem.* **284,** 2593–2597 CrossRef Medline
2. Carman, G. M., and Han, G. S. (2019) Fat-regulating phosphatidic acid phosphatase: a review of its roles and regulation in lipid homeostasis. *J. Lipid Res.* **60,** 2–6 CrossRef Medline
3. Carman, G. M. (2019) Discoveries of the phosphatidate phosphatase genes in yeast. *J. Biol. Chem.* **294,** 1681–1689 CrossRef Medline
4. Kwiatek, J. M., Han, G. S., and Carman, G. M. (2020) Phosphatidate-mediated regulation of lipid synthesis at the nuclear/endoplasmic reticulum membrane. *Biochim. Biophys. Acta* **1865,** 158434 CrossRef Medline
5. Carman, G. M., and Henry, S. A. (1989) Phospholipid biosynthesis in yeast. *Annu. Rev. Biochem.* **58,** 635–669 CrossRef Medline
6. Carman, G. M., and Henry, S. A. (1999) Phospholipid biosynthesis in the yeast *Saccharomyces cerevisiae* and interrelationship with other metabolic processes. *Prog. Lipid Res.* **38,** 361–399 CrossRef Medline
7. Henry, S. A., Kohlwein, S., and Carman, G. M. (2012) Metabolism and regulation of glycerolipids in the yeast *Saccharomyces cerevisiae. Genetics* **190,** 317–349 CrossRef Medline
8. Carman, G. M., and Han, G.-S. (2006) Roles of phosphatidate phosphatase enzymes in lipid metabolism. *Trends Biochem. Sci.* **31,** 694–699 CrossRef Medline
9. Pascual, F., and Carman, G. M. (2013) Phosphatidate phosphatase, a key regulator of lipid homeostasis. *Biochim. Biophys. Acta* **1831,** 514–522 CrossRef Medline
10. Han, G.-S., Wu, W.-I., and Carman, G. M. (2006) The *Saccharomyces cerevisiae* lipin homolog is a Mg^{2+}-dependent phosphatidate phosphatase enzyme. *J. Biol. Chem.* **281,** 9210–9218 CrossRef Medline
11. Lin, Y.-P., and Carman, G. M. (1989) Purification and characterization of phosphatidate phosphatase from *Saccharomyces cerevisiae. J. Biol. Chem.* **264,** 8641–8645 Medline
12. Smith, S. W., Weiss, S. B., and Kennedy, E. P. (1957) The enzymatic dephosphorylation of phosphatidic acids. *J. Biol. Chem.* **228,** 915–922 Medline
13. Choi, H.-S., Su, W.-M., Morgan, J. M., Han, G.-S., Xu, Z., Karanasios, E., Siniossoglou, S., and Carman, G. M. (2011) Phosphorylation of phosphatidate phosphatase regulates its membrane association and physiological functions in *Saccharomyces cerevisiae:* identification of Ser^{602}, Thr^{723}, and Ser^{744} as the sites phosphorylated by *CDC28 (CDK1)*-encoded

cyclin-dependent kinase. *J. Biol. Chem.* **286,** 1486–1498 CrossRef Medline

14. Choi, H.-S., Su, W.-M., Han, G.-S., Plote, D., Xu, Z., and Carman, G. M. (2012) Pho85p-Pho80p phosphorylation of yeast Pah1p phosphatidate phosphatase regulates its activity, location, abundance, and function in lipid metabolism. *J. Biol. Chem.* **287,** 11290–11301 CrossRef Medline

15. Su, W.-M., Han, G.-S., Casciano, J., and Carman, G. M. (2012) Protein kinase A-mediated phosphorylation of Pah1p phosphatidate phosphatase functions in conjunction with the Pho85p-Pho80p and Cdc28p-cyclin B kinases to regulate lipid synthesis in yeast. *J. Biol. Chem.* **287,** 33364–33376 CrossRef Medline

16. Su, W.-M., Han, G.-S., and Carman, G. M. (2014) Cross-talk phosphorylations by protein kinase C and Pho85p-Pho80p protein kinase regulate Pah1p phosphatidate phosphatase abundance in *Saccharomyces cerevisiae. J. Biol. Chem.* **289,** 18818–18830 CrossRef

17. Hsieh, L.-S., Su, W.-M., Han, G.-S., and Carman, G. M. (2016) Phosphorylation of yeast Pah1 phosphatidate phosphatase by casein kinase II regulates its function in lipid metabolism. *J. Biol. Chem.* **291,** 9974–9990 CrossRef Medline

18. Hassaninasab, A., Hsieh, L. S., Su, W. M., Han, G. S., and Carman, G. M. (2019) Yck1 casein kinase I regulates the activity and phosphorylation of Pah1 phosphatidate phosphatase from *Saccharomyces cerevisiae. J. Biol. Chem.* **294,** 18256–18268 CrossRef Medline

19. Gruhler, A., Olsen, J. V., Mohammed, S., Mortensen, P., Faergeman, N. J., Mann, M., and Jensen, O. N. (2005) Quantitative phosphoproteomics applied to the yeast pheromone signaling pathway. *Mol. Cell. Proteomics* **4,** 310–327 CrossRef Medline

20. O'Hara, L., Han, G.-S., Peak-Chew, S., Grimsey, N., Carman, G. M., and Siniossoglou, S. (2006) Control of phospholipid synthesis by phosphorylation of the yeast lipin Pah1p/Smp2p Mg^{2+}-dependent phosphatidate phosphatase. *J. Biol. Chem.* **281,** 34537–34548 CrossRef Medline

21. Li, X., Gerber, S. A., Rudner, A. D., Beausoleil, S. A., Haas, W., Villen, J., Elias, J. E., and Gygi, S. P. (2007) Large-scale phosphorylation analysis of alpha-factor-arrested *Saccharomyces cerevisiae. J. Proteome Res.* **6,** 1190–1197 CrossRef Medline

22. Chi, A., Huttenhower, C., Geer, L. Y., Coon, J. J., Syka, J. E., Bai, D. L., Shabanowitz, J., Burke, D. J., Troyanskaya, O. G., and Hunt, D. F. (2007) Analysis of phosphorylation sites on proteins from *Saccharomyces cerevisiae* by electron transfer dissociation (ETD) mass spectrometry. *Proc. Natl. Acad. Sci. U S A* **104,** 2193–2198 CrossRef

23. Smolka, M. B., Albuquerque, C. P., Chen, S. H., and Zhou, H. (2007) Proteome-wide identification of in vivo targets of DNA damage checkpoint kinases. *Proc. Natl. Acad. Sci. U S A* **104,** 10364–10369 CrossRef Medline

24. Albuquerque, C. P., Smolka, M. B., Payne, S. H., Bafna, V., Eng, J., and Zhou, H. (2008) A multidimensional chromatography technology for in-depth phosphoproteome analysis. *Mol. Cell. Proteomics* **7,** 1389–1396 CrossRef Medline

25. Soufi, B., Kelstrup, C. D., Stoehr, G., Frohlich, F., Walther, T. C., and Olsen, J. V. (2009) Global analysis of the yeast osmotic stress response by quantitative proteomics. *Mol. Biosyst.* **5,** 1337–1346 CrossRef Medline

26. Gnad, F., de Godoy, L. M., Cox, J., Neuhauser, N., Ren, S., Olsen, J. V., and Mann, M. (2009) High-accuracy identification and bioinformatic analysis of in vivo protein phosphorylation sites in yeast. *Proteomics* **9,** 4642–4652 CrossRef Medline

27. Helbig, A. O., Rosati, S., Pijnappel, P. W., van, B. B., Timmers, M. H., Mohammed, S., Slijper, M., and Heck, A. J. (2010) Perturbation of the yeast N-acetyltransferase NatB induces elevation of protein phosphorylation levels. *BMC Genomics* **11,** 685 CrossRef Medline

28. Soulard, A., Cremonesi, A., Moes, S., Schutz, F., Jeno, P., and Hall, M. N. (2010) The rapamycin-sensitive phosphoproteome reveals that TOR controls protein kinase A toward some but not all substrates. *Mol. Biol. Cell* **21,** 3475–3486 CrossRef Medline

29. Bodenmiller, B., Wanka, S., Kraft, C., Urban, J., Campbell, D., Pedrioli, P. G., Gerrits, B., Picotti, P., Lam, H., Vitek, O., Brusniak, M. Y., Roschitzki, B., Zhang, C., Shokat, K. M., Schlapbach, R., *et al.* (2010) Phosphoproteomic analysis reveals interconnected system-wide responses to perturbations of kinases and phosphatases in yeast. *Sci. Signal.* **3,** rs4 CrossRef Medline

30. Swaney, D. L., Beltrao, P., Starita, L., Guo, A., Rush, J., Fields, S., Krogan, N. J., and Villen, J. (2013) Global analysis of phosphorylation and ubiquitylation cross-talk in protein degradation. *Nat. Methods* **10,** 676–682 CrossRef Medline

31. Siniossoglou, S., Santos-Rosa, H., Rappsilber, J., Mann, M., and Hurt, E. (1998) A novel complex of membrane proteins required for formation of a spherical nucleus. *EMBO J.* **17,** 6449–6464 CrossRef Medline

32. Karanasios, E., Han, G.-S., Xu, Z., Carman, G. M., and Siniossoglou, S. (2010) A phosphorylation-regulated amphipathic helix controls the membrane translocation and function of the yeast phosphatidate phosphatase. *Proc. Natl. Acad. Sci. U S A* **107,** 17539–17544 CrossRef Medline

33. Karanasios, E., Barbosa, A. D., Sembongi, H., Mari, M., Han, G.-S., Reggiori, F., Carman, G. M., and Siniossoglou, S. (2013) Regulation of lipid droplet and membrane biogenesis by the acidic tail of the phosphatidate phosphatase Pah1p. *Mol. Biol. Cell* **24,** 2124–2133 CrossRef Medline

34. Su, W.-M., Han, G.-S., and Carman, G. M. (2014) Yeast Nem1-Spo7 protein phosphatase activity on Pah1 phosphatidate phosphatase is specific for the Pho85-Pho80 protein kinase phosphorylation sites. *J. Biol. Chem.* **289,** 34699–34708 CrossRef Medline

35. Pascual, F., Hsieh, L.-S., Soto-Cardalda, A., and Carman, G. M. (2014) Yeast Pah1p phosphatidate phosphatase is regulated by proteasome-mediated degradation. *J. Biol. Chem.* **289,** 9811–9822 CrossRef Medline

36. Hsieh, L.-S., Su, W.-M., Han, G.-S., and Carman, G. M. (2015) Phosphorylation regulates the ubiquitin-independent degradation of yeast Pah1 phosphatidate phosphatase by the 20S proteasome. *J. Biol. Chem.* **290,** 11467–11478 CrossRef Medline

37. Holt, L. J., Tuch, B. B., Villen, J., Johnson, A. D., Gygi, S. P., and Morgan, D. O. (2009) Global analysis of Cdk1 substrate phosphorylation sites provides insights into evolution. *Science* **325,** 1682–1686 CrossRef Medline

38. Dubots, E., Cottier, S., Peli-Gulli, M. P., Jaquenoud, M., Bontron, S., Schneiter, R., and De Virgilio, C. (2014) TORC1 regulates Pah1 phosphatidate phosphatase activity via the Nem1/Spo7 protein phosphatase complex. *PLoS. One* **9,** e104194 CrossRef Medline

39. Dey, P., Su, W. M., Han, G. S., and Carman, G. M. (2017) Phosphorylation of lipid metabolic enzymes by yeast Pkc1 protein kinase C requires phosphatidylserine and diacylglycerol. *J. Lipid Res.* **58,** 742–751 CrossRef Medline

40. Su, W.-M., Han, G. S., Dey, P., and Carman, G. M. (2018) Protein kinase A phosphorylates the Nem1-Spo7 protein phosphatase complex that regulates the phosphorylation state of the phosphatidate phosphatase Pah1 in yeast. *J. Biol. Chem.* **293,** 15801–15814 CrossRef Medline

41. Dey, P., Su, W. M., Mirheydari, M., Han, G. S., and Carman, G. M. (2019) Protein kinase C mediates the phosphorylation of the Nem1-Spo7 protein phosphatase complex in yeast. *J. Biol. Chem.* **294,** 15997–16009 CrossRef Medline

42. Han, G.-S., Siniossoglou, S., and Carman, G. M. (2007) The cellular functions of the yeast lipin homolog Pah1p are dependent on its phosphatidate phosphatase activity. *J. Biol. Chem.* **282,** 37026–37035 CrossRef Medline

43. Santos-Rosa, H., Leung, J., Grimsey, N., Peak-Chew, S., and Siniossoglou, S. (2005) The yeast lipin Smp2 couples phospholipid biosynthesis to nuclear membrane growth. *EMBO J.* **24,** 1931–1941 CrossRef Medline

44. Park, Y., Han, G. S., and Carman, G. M. (2017) A conserved tryptophan within the WRDPLVDID domain of yeast Pah1 phosphatidate phosphatase is required for its in vivo function in lipid metabolism. *J. Biol. Chem.* **292,** 19580–19589 CrossRef Medline

45. Irie, K., Takase, M., Araki, H., and Oshima, Y. (1993) A gene, *SMP2*, involved in plasmid maintenance and respiration in *Saccharomyces cerevisiae* encodes a highly charged protein. *Mol. Gen. Genet.* **236,** 283–288 CrossRef Medline

46. Korn, A. P., and Burnett, R. M. (1991) Distribution and complementarity of hydropathy in multisubunit proteins. *Proteins* **9,** 37–55 CrossRef Medline

47. Ghaemmaghami, S., Huh, W.-K., Bower, K., Howson, R. W., Belle, A., Dephoure, N., O'Shea, E. K., and Weissman, J. S. (2003) Global analysis of protein expression in yeast. *Nature* **425,** 737–741 CrossRef Medline

48. Pascual, F., Soto-Cardalda, A., and Carman, G. M. (2013) *PAH1*-encoded phosphatidate phosphatase plays a role in the growth phase- and inositol-mediated regulation of lipid synthesis in *Saccharomyces cerevisiae. J. Biol. Chem.* **288,** 35781–35792 CrossRef Medline

49. Adeyo, O., Horn, P. J., Lee, S., Binns, D. D., Chandrahas, A., Chapman, K. D., and Goodman, J. M. (2011) The yeast lipin orthologue Pah1p is important for biogenesis of lipid droplets. *J. Cell Biol.* **192,** 1043–1055 CrossRef Medline

50. Fakas, S., Qiu, Y., Dixon, J. L., Han, G.-S., Ruggles, K. V., Garbarino, J., Sturley, S. L., and Carman, G. M. (2011) Phosphatidate phosphatase activity plays a key role in protection against fatty acid-induced toxicity in yeast. *J. Biol. Chem.* **286,** 29074–29085 CrossRef Medline

51. Sasser, T., Qiu, Q. S., Karunakaran, S., Padolina, M., Reyes, A., Flood, B., Smith, S., Gonzales, C., and Fratti, R. A. (2012) The yeast lipin 1 orthologue Pah1p regulates vacuole homeostasis and membrane fusion. *J. Biol. Chem.* **287,** 2221–2236 CrossRef Medline

52. Xu, X., and Okamoto, K. (2018) The Nem1-Spo7 protein phosphatase complex is required for efficient mitophagy in yeast. *Biochem. Biophys. Res. Commun.* **496,** 51–57 CrossRef Medline

53. Rahman, M. A., Mostofa, M. G., and Ushimaru, T. (2018) The Nem1/Spo7-Pah1/lipin axis is required for autophagy induction after TORC1 inactivation. *FEBS J.* **285,** 1840–1860 CrossRef Medline

54. Han, G.-S., and Carman, G. M. (2017) Yeast *PAH1*-encoded phosphatidate phosphatase controls the expression of *CHO1*-encoded phosphatidylserine synthase for membrane phospholipid synthesis. *J. Biol. Chem.* **292,** 13230–13242 CrossRef Medline

55. Park, Y., Han, G. S., Mileykovskaya, E., Garrett, T. A., and Carman, G. M. (2015) Altered lipid synthesis by lack of yeast Pah1 phosphatidate phosphatase reduces chronological life span. *J. Biol. Chem.* **290,** 25382–25394 CrossRef Medline

56. Esposito, R. E., Frink, N., Bernstein, P., and Esposito, M. S. (1972) The genetic control of sporulation in *Saccharomyces*. II. Dominance and complementation of mutants of meiosis and spore formation. *Mol. Gen. Genet.* **114,** 241–248 CrossRef Medline

57. Fakas, S., Konstantinou, C., and Carman, G. M. (2011) *DGK1*-encoded diacylglycerol kinase activity is required for phospholipid synthesis during growth resumption from stationary phase in *Saccharomyces cerevisiae. J. Biol. Chem.* **286,** 1464–1474 CrossRef Medline

58. Kurat, C. F., Natter, K., Petschnigg, J., Wolinski, H., Scheuringer, K., Scholz, H., Zimmermann, R., Leber, R., Zechner, R., and Kohlwein, S. D. (2006) Obese yeast: triglyceride lipolysis is functionally conserved from mammals to yeast. *J. Biol. Chem.* **281,** 491–500 CrossRef Medline

59. Athenstaedt, K., and Daum, G. (2003) YMR313c/TGL3 encodes a novel triacylglycerol lipase located in lipid particles of *Saccharomyces cerevisiae. J. Biol. Chem.* **278,** 23317–23323 CrossRef Medline

60. Athenstaedt, K., and Daum, G. (2005) Tgl4p and Tgl5p, two triacylglycerol lipases of the yeast *Saccharomyces cerevisiae* are localized to lipid particles. *J. Biol. Chem.* **280,** 37301–37309 CrossRef Medline

61. Zanghellini, J., Natter, K., Jungreuthmayer, C., Thalhammer, A., Kurat, C. F., Gogg-Fassolter, G., Kohlwein, S. D., and von Grunberg, H. H. (2008) Quantitative modeling of triacylglycerol homeostasis in yeast–metabolic requirement for lipolysis to promote membrane lipid synthesis and cellular growth. *FEBS J.* **275,** 5552–5563 CrossRef Medline

62. Rajakumari, S., Grillitsch, K., and Daum, G. (2008) Synthesis and turnover of non-polar lipids in yeast. *Prog. Lipid Res.* **47,** 157–171 CrossRef Medline

63. Kohlwein, S. D. (2010) Triacylglycerol homeostasis: insights from yeast. *J. Biol. Chem.* **285,** 15663–15667 CrossRef Medline

64. Kudo, S., Shiino, H., Furuta, S., and Tamura, Y. (2020) Yeast transformation stress, together with loss of Pah1, phosphatidic acid phosphatase, leads to Ty1 retrotransposon insertion into the INO4 gene. *FASEB J.* **34,** 4749–4763 CrossRef Medline

65. Han, S., Bahmanyar, S., Zhang, P., Grishin, N., Oegema, K., Crooke, R., Graham, M., Reue, K., Dixon, J. E., and Goodman, J. M. (2012) Nuclear envelope phosphatase 1-regulatory subunit 1 (formerly TMEM188) is the metazoan Spo7p ortholog and functions in the lipin activation pathway. *J. Biol. Chem.* **287,** 3123–3137 CrossRef Medline

66. Tsai, C. J., Lin, S. L., Wolfson, H. J., and Nussinov, R. (1997) Studies of protein-protein interfaces: a statistical analysis of the hydrophobic effect. *Protein Sci.* **6,** 53–64 CrossRef Medline

67. Kim, Y., Gentry, M. S., Harris, T. E., Wiley, S. E., Lawrence, J. C., Jr., and Dixon, J. E. (2007) A conserved phosphatase cascade that regulates nuclear membrane biogenesis. *Proc. Natl. Acad. Sci. U S A* **104,** 6596–6601 CrossRef Medline

68. Péterfy, M., Phan, J., Xu, P., and Reue, K. (2001) Lipodystrophy in the *fld* mouse results from mutation of a new gene encoding a nuclear protein, lipin. *Nat. Genet.* **27,** 121–124 CrossRef Medline

69. Donkor, J., Sariahmetoglu, M., Dewald, J., Brindley, D. N., and Reue, K. (2007) Three mammalian lipins act as phosphatidate phosphatases with distinct tissue expression patterns. *J. Biol. Chem.* **282,** 3450–3457 CrossRef Medline

70. Han, G.-S., and Carman, G. M. (2010) Characterization of the human *LPIN1*-encoded phosphatidate phosphatase isoforms. *J. Biol. Chem.* **285,** 14628–14638 CrossRef Medline

71. Brindley, D. N. (1984) Intracellular translocation of phosphatidate phosphohydrolase and its possible role in the control of glycerolipid synthesis. *Prog. Lipid Res.* **23,** 115–133 CrossRef Medline

72. Cascales, C., Bosca, L., Martin, A., Brindley, D. N., and Cascales, M. (1988) Age-related changes in the translocation of phosphatidate phosphatase from the cytosol to microsomal membranes in rat liver. *Biochim. Biophys. Acta* **963,** 384–388 CrossRef Medline

73. Cascales, C., Mangiapane, E. H., and Brindley, D. N. (1984) Oleic acid promotes the activation and translocation of phosphatidate phosphatase. *Biochem. J.* **219,** 911–916 CrossRef Medline

74. Eaton, J. M., Mullins, G. R., Brindley, D. N., and Harris, T. E. (2013) Phosphorylation of lipin 1 and charge on the phosphatidic acid head group control its phosphatidic acid phosphatase activity and membrane association. *J. Biol. Chem.* **288,** 9933–9945 CrossRef Medline

75. Harris, T. E., Huffman, T. A., Chi, A., Shabanowitz, J., Hunt, D. F., Kumar, A., and Lawrence, J. C. Jr. (2007) Insulin controls subcellular localization and multisite phosphorylation of the phosphatidic acid phosphatase, lipin 1. *J. Biol. Chem.* **282,** 277–286. CrossRef Medline

76. Peterson, T. R., Sengupta, S. S., Harris, T. E., Carmack, A. E., Kang, S. A., Balderas, E., Guertin, D. A., Madden, K. L., Carpenter, A. E., Finck, B. N., and Sabatini, D. M. (2011) mTOR complex 1 regulates lipin 1 localization to control the SREBP pathway. *Cell* **146,** 408–420 CrossRef Medline

77. Zanivan, S., Gnad, F., Wickstrom, S. A., Geiger, T., Macek, B., Cox, J., Fassler, R., and Mann, M. (2008) Solid tumor proteome and phosphoproteome analysis by high resolution mass spectrometry. *J. Proteome Res.* **7,** 5314–5326 CrossRef Medline

78. Grimsrud, P. A., Carson, J. J., Hebert, A. S., Hubler, S. L., Niemi, N. M., Bailey, D. J., Jochem, A., Stapleton, D. S., Keller, M. P., Westphall, M. S., Yandell, B. S., Attie, A. D., Coon, J. J., and Pagliarini, D. J. (2012) A quantitative map of the liver mitochondrial phosphoproteome reveals posttranslational control of ketogenesis. *Cell Metab.* **16,** 672–683 CrossRef Medline

79. Humphrey, S. J., Yang, G., Yang, P., Fazakerley, D. J., Stockli, J., Yang, J. Y., and James, D. E. (2013) Dynamic adipocyte phosphoproteome reveals that Akt directly regulates mTORC2. *Cell Metab.* **17,** 1009–1020 CrossRef Medline

80. Lundby, A., Andersen, M. N., Steffensen, A. B., Horn, H., Kelstrup, C. D., Francavilla, C., Jensen, L. J., Schmitt, N., Thomsen, M. B., and Olsen, J. V. (2013) *In vivo* phosphoproteomics analysis reveals the cardiac targets of b-adrenergic receptor signaling. *Sci. Signal.* **6,** rs11 CrossRef Medline

81. Hennessy, M., Granade, M. E., Hassaninasab, A., Wang, D., Kwiatek, J. M., Han, G.-S., Harris, T. E., and Carman, G. M. (2019) Casein kinase II-mediated phosphorylation of lipin 1b phosphatidate phosphatase at Ser-285 and Ser-287 regulates its interaction with 14-3-3b protein. *J. Biol. Chem.* **294,** 2365–2374 CrossRef

82. Wu, R., Garland, M., Dunaway-Mariano, D., and Allen, K. N. (2011) *Homo sapiens* Dullard protein phosphatase shows a preference for the insulin-dependent phosphorylation site of lipin1. *Biochemistry* **50,** 3045–3047 CrossRef Medline

83. Zeharia, A., Shaag, A., Houtkooper, R. H., Hindi, T., de, L. P., Erez, G., Hubert, L., Saada, A., de, K. Y., Eshel, G., Vaz, F. M., Pines, O., and

ASBMB

Elpeleg, O. (2008) Mutations in *LPIN1* cause recurrent acute myoglobinuria in childhood. *Am. J. Hum. Genet.* **83,** 489–494 CrossRef Medline

84. Zhang, P., Verity, M. A., and Reue, K. (2014) Lipin-1 regulates autophagy clearance and intersects with statin drug effects in skeletal muscle. *Cell Metab.* **20,** 267–279 CrossRef Medline

85. Nadra, K., De Preux Charles, A.-S., Medard, J.-J., Hendriks, W. T., Han, G.-S., Gres, S., Carman, G. M., Saulnier-Blache, J.-S., Verheijen, M. H. G., and Chrast, R. (2008) Phosphatidic acid mediates demyelination in *Lpin1* mutant mice. *Genes Dev.* **22,** 1647–1661 CrossRef Medline

86. Wiedmann, S., Fischer, M., Koehler, M., Neureuther, K., Riegger, G., Doering, A., Schunkert, H., Hengstenberg, C., and Baessler, A. (2008) Genetic variants within the *LPIN1* gene, encoding lipin, are influencing phenotypes of the metabolic syndrome in humans. *Diabetes* **57,** 209–217 CrossRef Medline

87. Ferguson, P. J., and El-Shanti, H. I. (2007) Autoinflammatory bone disorders. *Curr. Opin. Rheumatol.* **19,** 492–498 CrossRef

88. Ferguson, P. J., Chen, S., Tayeh, M. K., Ochoa, L., Leal, S. M., Pelet, A., Munnich, A., Lyonnet, S., Majeed, H. A., and El-Shanti, H. (2005) Homozygous mutations in *LPIN2* are responsible for the syndrome of chronic recurrent multifocal osteomyelitis and congenital dyserythropoietic anaemia (Majeed syndrome). *J. Med. Genet.* **42,** 551–557 CrossRef Medline

89. Aulchenko, Y. S., Pullen, J., Kloosterman, W. P., Yazdanpanah, M., Hofman, A., Vaessen, N., Snijders, P. J. L. M., Zubakov, D., Mackay, I., Olavesen, M., Sidhu, B., Smith, V. E., Carey, A., Berezikov, E., Uitterlinden, A. G., *et al.* (2007) *LPIN2* is associated with type 2 diabetes, glucose metabolism and body composition. *Diabetes* **56,** 3020–3026 CrossRef

90. Zhang, P., Csaki, L. S., Ronquillo, E., Baufeld, L. J., Lin, J. Y., Gutierrez, A., Dwyer, J. R., Brindley, D. N., Fong, L. G., Tontonoz, P., Young, S. G., and Reue, K. (2019) Lipin 2/3 phosphatidic acid phosphatases maintain phospholipid homeostasis to regulate chylomicron synthesis. *J. Clin. Invest.* **129,** 281–295 CrossRef Medline

91. Hayata, T., Chiga, M., Ezura, Y., Asashima, M., Katabuchi, H., Nishinakamura, R., and Noda, M. (2018) Dullard deficiency causes hemorrhage in the adult ovarian follicles. *Genes Cells* **23,** 345–356 CrossRef Medline

92. Sikorski, R. S., and Hieter, P. (1989) A system of shuttle vectors and yeast host strains designed for efficient manipulation of DNA in *Saccharomyces cerevisiae*. *Genetics* **122,** 19–27 Medline

93. Han, G.-S., O'Hara, L., Carman, G. M., and Siniossoglou, S. (2008) An unconventional diacylglycerol kinase that regulates phospholipid synthesis and nuclear membrane growth. *J. Biol. Chem.* **283,** 20433–20442 CrossRef Medline

94. Rose, M. D., Winston, F., and Heiter, P. (1990) *Methods in Yeast Genetics: A Laboratory Course Manual*, Cold Spring Harbor Laboratory Press, Cold Spring Harbor, NY

95. Sambrook, J., Fritsch, E. F., and Maniatis, T. (1989) *Molecular Cloning, A Laboratory Manual*, 2nd Ed., Cold Spring Harbor Laboratory, Cold Spring Harbor, NY

96. Innis, M. A., Gelfand, D. H. (1990) *PCR Protocols: A Guide to Methods and Applications* (Innis, M. A., Gelfand, D. H., Sninsky, J. J., and White, T. J., eds) pp. 3–12, Academic Press, Inc., San Diego, CA

97. Ito, H., Fukuda, Y., Murata, K., and Kimura, A. (1983) Transformation of intact yeast cells treated with alkali cations. *J. Bacteriol.* **153,** 163–168 CrossRef Medline

98. Carman, G. M., and Lin, Y.-P. (1991) Phosphatidate phosphatase from yeast. *Methods Enzymol.* **197,** 548–553 CrossRef Medline

99. Bradford, M. M. (1976) A rapid and sensitive method for the quantitation of microgram quantities of protein utilizing the principle of protein-dye binding. *Anal. Biochem.* **72,** 248–254 CrossRef Medline

100. Harlow, E., and Lane, D. (1988) *Antibodies. A Laboratory Manual*, Cold Spring Harbor Laboratory Press, Cold Spring Harbor, NY

101. Laemmli, U. K. (1970) Cleavage of structural proteins during the assembly of the head of bacteriophage T4. *Nature* **227,** 680–685 CrossRef Medline

102. Guengerich, F. P., Wang, P., and Davidson, N. K. (1982) Estimation of isozymes of microsomal cytochrome P-450 in rats, rabbits, and humans using immunochemical staining coupled with sodium dodecyl sulfate-polyacrylamide gel electrophoresis. *Biochemistry* **21,** 1698–1706 CrossRef Medline

103. Burnette, W. (1981) Western blotting: electrophoretic transfer of proteins from sodium dodecyl sulfate-polyacrylamide gels to unmodified nitrocellulose and radiographic detection with antibody and radioiodinated protein A. *Anal. Biochem.* **112,** 195–203 CrossRef Medline

104. Haid, A., and Suissa, M. (1983) Immunochemical identification of membrane proteins after sodium dodecyl sulfate-polyacrylamide gel electrophoresis. *Methods Enzymol.* **96,** 192–205 CrossRef Medline

105. Morlock, K. R., Lin, Y.-P., and Carman, G. M. (1988) Regulation of phosphatidate phosphatase activity by inositol in *Saccharomyces cerevisiae*. *J. Bacteriol.* **170,** 3561–3566 CrossRef Medline

106. Bligh, E. G., and Dyer, W. J. (1959) A rapid method of total lipid extraction and purification. *Can. J. Biochem. Physiol.* **37,** 911–917 CrossRef Medline

107. Henderson, R. J., and Tocher, D. R. (1992) *Lipid Analysis* (Hamilton, R. J., and Hamilton, S., eds) pp. 65–111, IRL Press, New York

108. Vida, T. A., and Emr, S. D. (1995) A new vital stain for visualizing vacuolar membrane dynamics and endocytosis in yeast. *J. Cell Biol.* **128,** 779–792 CrossRef Medline

109. Soto-Cardalda, A., Fakas, S., Pascual, F., Choi, H. S., and Carman, G. M. (2012) Phosphatidate phosphatase plays role in zinc-mediated regulation of phospholipid synthesis in yeast. *J. Biol. Chem.* **287,** 968–977 CrossRef Medline

110. Carman, G. M., and Han, G.-S. (2011) Regulation of phospholipid synthesis in the yeast *Saccharomyces cerevisiae*. *Ann. Rev. Biochem.* **80,** 859–883 CrossRef Medline

🔬 ASBMB

J. Biol. Chem. (2020) 295(33) 11473–11485 **11485**